Relaxation of spin quantum number $S=3/2$ under multiple-pulse quadrupolar echoes

J. R. C. van der Maarel
Department of Physical and Macromolecular Chemistry, Gorlaeus Laboratories, University of Leiden, P.O. Box 9502, 2300 RA Leiden, The Netherlands

(Received 9 August 1990; accepted 4 December 1990)

The time evolution of the spin $S = 3/2$ density operator due to relaxation in the presence of a sequence of $(\pi/2)$ pulses has been calculated using perturbation theory in an interaction representation in which no external time-dependent rf fields occur. It is shown that the relaxation under the effect of the pulse train is similar to $T_{1\rho}$ relaxation. If the magnetization is sampled between the pulses, outside extreme narrowing conditions the observed signal is characterized by a biexponential decay. The amplitude ratio of the fast and slowly relaxing component equals 0.8:0.2. The rate of the fast relaxing component is sensitive to the pulse cycle time in the presence of slowly fluctuating electric-field gradients. A full expression of the relevant spectral density function valid for $(\pi/2)$ pulses with arbitrary pulse width has been derived. In this derivation, the processes involved in determining the loss of correlation of the quadrupolar interaction are assumed to be independent and characterized by exponential correlation functions. Due to relaxation under the effect of the $(\pi/2)$ pulse train triple-quantum coherences may be excited. The latter coherences can be monitored by applying an additional coherence transfer pulse after the pulse train. The relaxation of sodium in an ion exchange resin in the presence of the $(\pi/2)$ pulse sequence has experimentally been studied and agrees with the theoretical analysis.

INTRODUCTION

Spin quantum number $S = 3/2$ NMR is an important probe to investigate the intricate behavior of small ions in a wide variety of condensed matter. Examples of these systems are synthetic and biological polymer solutions,[1,2] ionic conductors,[3] and other biological systems.[4] The most important spin $S = 3/2$ nuclei are ^{7}Li, ^{23}Na, ^{87}Rb, ^{35}Cl, and ^{81}Br. For these nuclei, the dominant relaxation mechanism is the electric quadrupolar interaction. Quadrupolar relaxation is determined by the magnitude and temporal duration of electric-field-gradients generated by the surrounding medium. Longitudinal and transverse magnetic relaxation experiments are sensitive to the spectral density of these fluctuations at zero, one, and two times the Larmor frequency with respect to the static field H_0. At the present-day laboratory field strengths this Larmor frequency is usually of the order of MHz. In many complex (macromolecular) systems, the characteristic correlation times of the electric-field-gradient fluctuations may be relatively long. Accordingly, the corresponding spectral density function may show a dispersion at frequencies far below the relatively high Larmor frequency. In this situation, transverse relaxation gives access to the zero-frequency component of this dispersion only.

The $T_{1\rho}$ experiment is sensitive to the spectral density at two times the precession frequency with respect to the spin-lock field. The latter frequency is of the order of kHz and depends on the transmitter power level. Accordingly, the spin-lock experiment may yield information about slowly fluctuating processes. In a previous communication, the time evolution of the spin $S = 3/2$ density operator under spin-locking has been analyzed.[5] It was shown that outside the extreme narrowing limit the relaxation becomes biexponential. Furthermore, due to this relaxation triple-quantum coherences are excited. Similar behavior has been reported for longitudinal and transverse relaxation experiments.[6,7] The resulting theoretical expressions describing the relaxation behavior under spin-locking have experimentally been verified in Ref. 8.

However, the continuous spin-lock experiment is characterized by a number of experimental drawbacks. The signal has to be detected as a function of the spin-lock time in a subsequent manner. Accordingly, a considerable amount of spectrometer time is involved. In the present contribution it will be shown that for spin $S = 3/2$ quadrupolar relaxation the spin-lock irradiation can be replaced by a $(\pi/2)$ pulse train. In this pulsed experiment the signal can be sampled between the pulses, and, hence, the relaxation curve is recorded in one scan. Another problem is the variation of the H_1 power level to probe the spectral density at two times the precession frequency with respect to the spin-lock field. A simultaneous power level and phase switch between the preparation pulse and the spin-lock field is electronically difficult to achieve. In the pulsed experiment the corresponding parameter is the pulse cycle time, which can easily be varied.

The applicability of the $(\pi/2)$ pulse train (Mansfield-Ware MW-4 sequence) to study dipolar relaxation in solids has been analyzed by several authors.[9-11] For a comprehensive review the reader is referred to the book by Mehring.[12] Quadrupolar relaxation has been treated by Blicharski.[13] However, in the latter contribution the discussion was confined to spin $S = 1$ in the limit of δ-function pulses. Recently, Vega, Poupko, and Luz analyzed the $(\pi/2)$ pulse train for spin $S = 1$ in a static field gradient undergoing exchange in a liquid-crystalline solvent.[14] They reported a full expression of the pulse spacing dependent relaxation rate valid for

 0021-9606/91/074765-11$03.00

$(\pi/2)$ pulses with arbitrary pulse width. Rhim, Burum, and Elleman[10] and Vega and Vaughan[11] reported similar equations, but for dipolar relaxation in solids.

In the present contribution, relaxation under the $(\pi/2)$ pulse train will be analyzed for spin $S=3/2$ quadrupolar relaxation. This experiment is similar to the Carr–Purcell–Gill–Meiboom (CPGM) pulse train, but with $(\pi/2)$ vs (π) pulses. In the latter experiment, shift-like (linear in the spin operator) terms in the Hamiltonian such as the scalar interaction between unlike spins are sign reversed by every (π) pulse. In a similar way, for a second-rank quadrupolar or dipolar interaction the relevant terms [i.e., the terms involving $m=0, k=\pm 2$ in Eq. (2) below] in the coupling Hamiltonian can be sign modulated by a $(\pi/2)$ pulse train. Accordingly, the latter experiment is sometimes referred to as the quadrupolar echo train experiment.[14] This sign modulation results in pulse cycle time-dependent relaxation rates provided the time scale of the slowly fluctuating interaction to be of the order of the cycle time. The time evolution of the density operator will be calculated using perturbation (Redfield) theory in an interaction representation in which no external time-dependent rf fields occur. The method follows closely the formalism used for the description of CPGM experiments in the presence of chemical exchange.[15] For the quadrupolar interaction mechanism, the characteristic relaxation times can be relatively short of the order of milliseconds. Accordingly, it may be necessary to use relatively short cycle times and the effect of the finite pulse width has to be taken into account.[14]

Using a convenient interaction representation it is shown that the relaxation under the $(\pi/2)$ pulse train is similar to $T_{1\rho}$ relaxation. The relaxation is biexponential (outside the extreme narrowing limit) and the rate of the fast relaxing component may be sensitive to the pulse cycle time. An explicit expression of the cycle time and pulse-width-dependent spectral density function will be derived, assuming an exponential correlation function. Due to relaxation during the pulse train triple-quantum coherences are generated. These coherences may be monitored in a similar manner as in the previously discussed spin-lock experiment with coherence transfer.[5] Some experimental results are presented which confirm the present analysis and the similarity of the spin-lock and quadrupolar echo train experiments. Finally, the conclusions are summarized and both experimental approaches are compared.

In the present contribution extensive use will be made of irreducible tensor operators in the context of relaxation and coherence transfer. This formalism has extensively been used in the papers by Jaccard, Wimperis, and Bodenhausen[7] and the present author.[5,16] Accordingly, for a description of the formalism the reader is referred to these papers.

RELAXATION DIFFERENTIAL EQUATION

The quadrupolar echo analog of the CPGM experiment can be represented by the pulse sequence: $(\pi/2)_y - [T/2 - (\pi/2)_x - T/2]_n$. To prepare the spin system, the magnetization is transferred to the $+x$ axis by an initial $(\pi/2)_y$ pulse. After this initial pulse, the density operator is represented by

$$\sigma^*(t=0) = S_x = (\tfrac{5}{2})^{1/2}(T_{1-1} - T_{1+1}) \tag{1}$$

in which the asterisk refers to the Larmor frequency rotating frame. Factors expressing the number of spins and the temperature have been dropped, since they are irrelevant for the present analysis. The unit tensor operators T_{lm} are normalized according to

$$\mathrm{Tr}\{T_{lm}T^{\dagger}_{l'm'}\} = \delta_{ll'}\delta_{mm'} \quad \text{with} \quad T^{\dagger}_{lm} = (-1)^m T_{l-m}.$$

After the magnetization has been transferred to the $+x$ axis a train of equal $(\pi/2)_x$ pulses is applied. This experiment is a pulsed version of the spin-lock experiment and is sometimes referred to as pulsed spin-locking.[10] The time dependence of the density operator under the influence of this pulsed spin-lock field has to be calculated. This is most conveniently performed in an interaction representation in which no external time-dependent rf fields occur. This interaction representation is a pulsed version of the doubly rotating tilted frame, which has previously been used to describe continuous spin-locking.[5,17] However, in the pulsed spin-lock experiment the amplitude of the applied H_1 field is time dependent, which leads to a modification of the transformation matrix. This interaction representation is referred to as the rotating tilted toggling frame (RTTF).

The present interaction representation is a simplified version of the well-known "nodding" frame.[18,19] The latter frame was originally devised to describe pulse sequences such as the four pulse sequence WAHUHA and derivatives thereof. In these pulse sequences the external H_1 field is both phase and amplitude modulated. In the interaction representation, the fluctuating interaction Hamiltonian is written in terms of switch functions to take into account the phase and amplitude modulation of the applied rf. Subsequently, these switch functions are expanded into Fourier series to calculate the relaxation using a perturbation analysis.[18] In the present situation, the pulse train is given along the $+x$-axis (amplitude modulation only). In the absence of rf phase modulation, the effect of the irradiation can be translated into a time-modulated argument of the Wigner transformation matrix.

In the RTTF (indicated by the double asterisk), the quadrupolar coupling Hamiltonian $\mathscr{H}_Q^{**}$ reads

$$\mathscr{H}_Q^{**}(t) = C \sum_{m,k=-2}^{2} (-1)^m T_{2k} \times D^{(2)}_{km}\left[-\int_0^t dt'\omega_1(t'), -\pi/2, -\omega_0 t\right] F_{2-m}. \tag{2}$$

In this expression $C = 3eQ/[S(2S-1)\hbar]$, T_{2k} denotes the nuclear-spin operator, and the field gradient tensor is given by F_{2m}.[20,21] The field gradient tensor elements read as $F_{20} = (1/2)V_{zz}$, $F_{2\pm 1} = \mp(6^{-1/2})(V_{xz} \pm iV_{yz})$, and $F_{2\pm 2} = (6^{-1/2}/2)(V_{xx} - V_{yy} \pm 2iV_{xy})$. The Wigner matrix transforms the (laboratory frame defined) spin-operator tensor T_{2k} to the RTTF. In this transformation $\omega_0 = -\gamma H_0$, $\omega_1(t) = -\gamma H_1(t)$, and it is implicitly assumed that the angle between the direction of the Zeeman field H_0 and the pulsed H_1 field equals $\pi/2$. Furthermore, the offset of the pulse carrier frequency from exact resonance

equals zero. The $H_1(t)$ field is applied exactly on resonance. In the Wigner matrix argument the sign and angle conventions of Rose are adopted.[22]

The difference between the doubly rotating tilted frame and the RTTF can be traced back to the Wigner matrix argument in Eq. (2). In the spin-lock experiment one applies a continuous H_1 field and the integral $\int_0^t dt'\,\omega_1(t')$ simply reduces to $\omega_1 t$. Substituting this value into Eq. (2), one recovers the corresponding Eq. (A2) in Ref. 5 for the continuous spin-lock case.

The time-dependent $\omega_1(t)$ is schematically depicted in Fig. 1(a), in which the various time intervals are defined. The time-dependent $\omega_1(t)$ is periodic in the cycle time T,

$$\omega_1(t)=\omega_1(nT+t_0)=\omega_1(t_0), \tag{3}$$

in which t_0 denotes the time elapsed after the nth echo. Accordingly, t_0 is defined in the time interval $0\leqslant t_0<T$. The time integral of $\omega_1(t)$ can be computed step by step for each time period. (An alternative is to expand the periodical irradiation into a Fourier series which can subsequently be integrated term by term.) The result is given by

$$\int_{t_a}^{t_b} dt'\,\omega_1(t')=\left[\frac{\pi t}{2T}+\frac{\pi}{4}\frac{1-\delta}{\delta}S(t)\right]\Bigg|_{t_a}^{t_b} \tag{4}$$

with the duty cycle parameter defined as $\delta=\tau_p/T$, $0<\delta\leqslant 1$. The first term on the right-hand side of Eq. (4) denotes the average value, whereas the second term accounts for the periodicity in the irradiation. Accordingly, in the limiting case of continuous spin-locking the latter term reduces to zero. The function $S(t)$ is depicted in Fig. 1(b) and is periodic in the cycle time T:

$$S(t)=S(nT+t_0)=S(t_0). \tag{5}$$

In the first period the function $S(t_0)$ reads

$$S(t_0)=\begin{cases}\dfrac{-2}{T}\dfrac{\delta}{1-\delta}t_0, & 0\leqslant t_0\leqslant (T-\tau_p)/2\\[2ex] -1+\dfrac{2}{T}t_0, & (T-\tau_p)/2\leqslant t_0\leqslant (T+\tau_p)/2\\[2ex] \dfrac{2\delta}{1-\delta}-\dfrac{2}{T}\dfrac{\delta}{1-\delta}t_0, & (T+\tau_p)/2\leqslant t_0<T.\end{cases} \tag{6}$$

To evaluate the time evolution of the spin system during the $(\pi/2)_x$ pulse train, the density operator in the Larmor frequency rotating frame [Eq. (1)] has to be transformed to the RTTF. If the general form of the density operator in the rotating frame is

$$\sigma^*=\sum_{l,m} c_{lm}T_{lm}, \tag{7}$$

then in the RTTF the density operator is represented by

$$\sigma^{**}=\sum_{k,l,m} c_{lm}T_{lk}D^{(l)}_{km}\left[-\int_0^t dt'\,\omega_1(t'),-\pi/2,0\right]. \tag{8}$$

Transforming Eq. (1) into the RTTF, one obtains according to Eq. (7) and (8)

$$\sigma^{**}(t=0)=5^{1/2}T_{10}. \tag{9}$$

The magnetization is along the z axis of the toggling frame. Accordingly, in the RTTF the density operator contains the T_{10} tensor component only.

During the $(\pi/2)_x$ pulse train, the density operator evolves due to relaxation. In the RTTF, where no external rf fields appear, the time dependence of the density operator can be evaluated using the well-known perturbation equation[23]

$$\frac{d\sigma^{**}}{dt}=-\int_0^\infty d\tau\langle[\mathscr{H}_Q^{**}(t),[\mathscr{H}_Q^{**}(t-\tau),\sigma^{**}(t)]]\rangle. \tag{10}$$

The conditions for the validity of Eq. (10) have been discussed by Abragam.[23] Substituting Eq. (2) into (10), then yields

$$\begin{aligned}\frac{d\sigma^{**}}{dt}=&-C^2\sum_{\substack{m,k,\\ m',k'=-2}}^{2}(-1)^{m+m'}\exp\left\{i\left[(m+m')\omega_0 t+(k+k')\int_0^t dt'\,\omega_1(t')\right]\right\}\\ &\times[T_{2k},[T_{2k'},\sigma^{**}]]d^{(2)}_{km}(-\pi/2)d^{(2)}_{k'm'}(-\pi/2)\\ &\times\int_0^\infty d\tau\langle F_{2-m}(t)F_{2-m'}(t-\tau)\rangle\exp\left\{-i\left[m'\omega_0\tau+k'\int_{t-\tau}^t dt'\,\omega_1(t')\right]\right\}.\end{aligned} \tag{11}$$

In Eq. (11) the nonsecular terms with $m\neq -m'$ are unimportant, because these terms oscillate with frequencies $(m+m')\omega_0$.[23] The only important terms involving k and k' are those for which the exponential $\exp[i(k+k')\int_0^t dt'\,\omega_1(t')]$ equals unity for all times t. Inserting the time integral of $\omega_1(t')$ [Eq. (4)], together with Eq. (5) and with $t=nT+t_0$, this exponential reduces to

$$\exp\left\{i(k+k')\frac{\pi}{2}\left[n+\frac{t_0}{T}+\frac{1-\delta}{2\delta}S(t_0)\right]\right\}. \tag{12}$$

With $k+k'=0$ this exponential equals unity for all times, irrespective of the pulse width τ_p. However, in the δ-function pulses limit, this exponential equals unity with $k+k'=\pm 4$ too. If the finite pulse width is not negligible, the exponential with $k+k'=\pm 4$ becomes time dependent

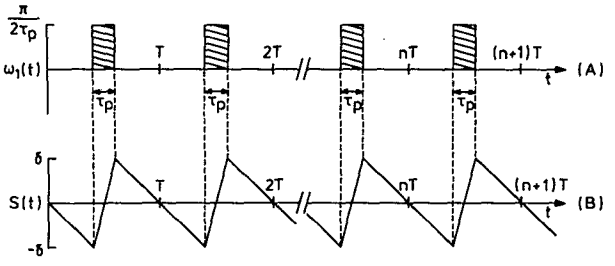

FIG. 1. (A) Schematic representation of $\omega_1(t) = -\gamma H_1(t)$. (B) Schematic representation of the function $S(t)$ defined by Eqs. (5) and (6).

during the pulse. The remaining terms are unimportant since they modulate the right-hand side of Eq. (11) at a frequency of the order $1/T$. Furthermore, in the Appendix it is shown that in the latter equation the terms involving odd values of $k+k'$ vanish. This is due to the symmetry properties of the reduced Wigner matrix elements and the condition Eq. (19) derived below.

It can be shown that for spin $S=3/2$ the terms involving $k+k' = \pm 4$ are unimportant even in the situation of δ-function pulses. This is most easily derived from the properties of the spin-operator double commutator.[21,22] The expansion of the density operator in irreducible tensors in Eq. (11) yields a set of equations in which the subset T_{10} and T_{30} is decoupled from any other T_{lm}. The double commutators reduce to combinations of $T_{lk+k'}$ which vanish when $k+k' = \pm 4$ and $S=3/2$.

As will become apparent shortly, the restriction to the secular terms with $k+k'=0$ will have an important consequence. Due to this restriction, the relaxation during the $(\pi/2)_x$ pulse train will be similar to $T_{1\rho}$ relaxation instead of T_2 relaxation, as one might intuitively expect. Both relaxation processes are characterized by a biexponential decay curve, but with different rates. Moreover, for $T_{1\rho}$ relaxation the amplitude ratio of the fast and slowly relaxing components equals 0.8:0.2, whereas for T_2 relaxation this corresponding ratio is given by 0.6:0.4.[5] Accordingly, it might be worthwhile to consider the situation for a Carr–Purcell–Gill–Meiboom transverse relaxation experiment using a pulse train consisting of $(\pi)_x$ pulses. In this situation, an equation similar to Eq. (12) can be derived, but with $\pi/2$ substituted by π. This expression equals unity for all times with $k+k'=0$ and, in the case of δ-function pulses, with $k+k' = \pm 2$ and $k+k' = \pm 4$. The terms involving $k+k' = \pm 4, \pm 2$ are responsible for the difference between transverse and $T_{1\rho}$ relaxation behavior. However, if the finite pulse width is not negligible, the latter terms will be gradually decoupled in the relaxation master Eq. (11), due to the spin-lock effect during the pulses. Consequently, the recorded CPGM decay curve will be more similar to the $T_{1\rho}$ instead of the transverse relaxation decay curve. This situation is very difficult to analyze and is beyond the scope of this contribution. However, due to this effect, for the determination of relatively short transverse relaxation times, the conventional spin-echo method is clearly to be preferred.

Restricting to the secular terms with $m=-m'$ and $k=-k'$, the differential equation describing the time evolution of the density operator reads

$$\frac{d\sigma^{**}}{dt} = -C^2 \sum_{k=-2}^{2} [T_{2k},[T_{2k}^{\dagger},\sigma^{**}]] \times \sum_{m=-2}^{2} |d_{km}^{(2)}(-\pi/2)|^2 \times \int_0^{\infty} d\tau \langle F_{2m}^{*}(t) F_{2m}(t-\tau)\rangle \times \exp\left\{ i\left[m\omega_0 \tau + k\int_{t-\tau}^{t} dt'\,\omega_1(t')\right]\right\}. \tag{13}$$

Using Eqs. (4) and (5), together with $t = nT + t_0$, it can been shown that $\int_{t-\tau}^{t} dt'\,\omega_1(t')$ is periodic in the cycle time T, i.e.,

$$\int_{t-\tau}^{t} dt'\,\omega_1(t') = \int_{t_0-\tau}^{t_0} dt'\,\omega_1(t'). \tag{14}$$

Generally, the signal will be stroboscopically sampled at the echo positions at times $t_n = nT$. Accordingly, the quantity of interest is given by

$$\frac{d\sigma^{**}}{dt_n} = \frac{\sigma^{**}([n+1]T) - \sigma^{**}([nT])}{T} = \frac{1}{T}\int_{nT}^{(n+1)T} dt \frac{d\sigma^{**}}{dt}. \tag{15}$$

The characteristic relaxation times are usually much longer than the cycle time T. Hence, the relative change in σ^{**} over the period T is assumed to be small:

$$\{[\sigma^{**}(nT+t_0) - \sigma^{**}(nT)]/\sigma^{**}(nT)\} \ll 1.$$

Inserting Eq. (13) into Eq. (15), together with Eq. (14) and the latter assumption, the desired differential equation for the stroboscopically sampled density operator takes the form

$$\frac{d\sigma^{**}}{dt_n} = -C^2 \sum_{k=-2}^{2} [T_{2k},[T_{2k}^{\dagger},\sigma^{**}]] \times \sum_{m=-2}^{2} |d_{km}^{(2)}(-\pi/2)|^2 J_{km}(T,m\omega_0) \tag{16}$$

with the pulse cycle time-dependent spectral densities

$$J_{km}(T,m\omega_0) = \frac{1}{2}\frac{1}{T}\int_0^T dt_0 \int_{-\infty}^{\infty} d\tau \langle F_{2m}^{*}(t) F_{2m}(t-\tau)\rangle \times \exp\left\{ i\left[m\omega_0\tau + k\int_{t_0-\tau}^{t_0} dt'\,\omega_1(t')\right]\right\}. \tag{17}$$

The imaginary part of the spectral density in Eq. (13) has been neglected. This part can be included in the unperturbed Zeeman Hamiltonian resulting in a very small second-order frequency shift.[23,24]

The relaxation differential Eq. (16) is exactly similar to the corresponding Eq. (A4) in Ref. 5 derived for the continuous spin-lock experiment, but with spectral densities $J_{km}(T,m\omega_0)$ vs $J_{km}(k\omega_1 + m\omega_0)$. The latter spectral den-

sity function refers to the continuous spin-lock case and is defined by Eq. (A5) in Ref. 5. As mentioned before, the similarity can be traced back to the restriction to the terms involving $k+k'=0$ in the original master relaxation Eq. (11) and Eq. (A3) in Ref. 5 for the pulsed and continuous spin-lock experiment, respectively. It will be shown below that in the limit of zero-pulse spacing $J_{km}(T,m\omega_0)$ will correctly reduce to $J_{km}(k\omega_1+m\omega_0)$. The expansion of the density operator over the irreducible tensors in Eq. (16) yields a set of equations which can be integrated. However, to evaluate the relaxation rates (eigenvalues) it is necessary to derive certain properties of the spectral density function $J_{km}(T,m\omega_0)$. Accordingly, in the next section this spectral density function will be evaluated as a function of the pulse cycle time and pulse width.

SPECTRAL DENSITY FUNCTION $J_{km}(T,m\omega_0)$

In the limit of zero-pulse spacing, ω_1 becomes time independent and the integral $\int_{t_0-\tau}^{t_0} dt'\,\omega_1(t')$ in Eq. (17) reduces to the simple quantity $\omega_1\tau$ with $\omega_1=\pi/2T$. In this situation the integral over the time integration variable t_0 can trivially be solved and the expression correctly reduces to

$$J_{km}(T,m\omega_0)=J_{km}(k\omega_1+m\omega_0)$$
$$=\frac{1}{2}\int_{-\infty}^{\infty} d\tau\langle F_{2m}^{*}(t)F_{2m}(t-\tau)\rangle$$
$$\times\exp[i(m\omega_0+k\omega_1)\tau]. \tag{18}$$

Another relatively simple situation occurs when the index $m\neq 0$. Since the (pulsed) H_1 field strength is generally much smaller than the static field strength H_0, for $m\neq 0$ one has the condition

$$m\omega_0 \gg k\frac{1}{\tau}\int_{t_0-\tau}^{t_0} dt'\,\omega_1(t') \quad \text{with } m\neq 0. \tag{19}$$

In this situation the integral over $\omega_1(t')$ in Eq. (17) can be neglected with respect to $m\omega_0$ and, again, the integral over integration variable t_0 can be dropped

$$J_{km}(T,m\omega_0)\approx J_m(m\omega_0)$$
$$=\frac{1}{2}\int_{-\infty}^{\infty} d\tau\langle F_{2m}^{*}(t)F_{2m}(t-\tau)\rangle$$
$$\times\exp\{im\omega_0\tau\}, \quad m\neq 0. \tag{20}$$

For $m=0$, the spectral density function has to be fully evaluated as a function of the cycle time T and the pulse width τ_p.

The only important spectral density function to be evaluated is $J_{20}(T)\,[=J_{-20}(T)]$. In the present analysis, the spectral density $J_{\pm 10}(T)\,[m=0,k=\pm 1]$ is irrelevant due to the zero value of the reduced Wigner matrix elements $[d^{(2)}_{\pm 10}(-\pi/2)=0]$. Furthermore, the spectral density $J_{00}\,[m=0,k=0]$ is irrelevant due to the commutation properties of the subset T_{10} and T_{30} in the set of relaxation equations Eq. (16). In $J_{20}(T)$ the correlation function is sign modulated due to the effect of the $(\pi/2)_x$ pulse train. Accordingly, a pulse cycle time-dependent relaxation rate is observed if the cycle time is of the order of the characteristic correlation time of the fluctuating interaction.

The spectral density function $J_{20}(T)$ will be evaluated assuming an exponential correlation function of the quadrupolar interaction

$$\langle F_{20}^{*}(t)F_{20}(t-\tau)\rangle = A\exp(-\tau/\tau_c)$$
$$\text{with } A=\tfrac{1}{20}(eq)^2(1+\eta^2/3). \tag{21}$$

In this equation τ_c denotes the correlation time, and eq and η are the principal value and asymmetry parameter of the electric-field-gradient tensor, respectively. Inserting Eq. (21), together with Eqs. (4) and (5) to evaluate the integral over $\omega_1(t')$ in Eq. (17), the spectral density function takes the form

$$J_{20}(T)=A\frac{1}{T}\int_0^T dt_0\ \mathrm{Re}\int_0^{\infty} d\tau\exp(-s\tau)$$
$$\times\exp\left\{i\pi\frac{1-\delta}{2\delta}[S(t_0)-S(t_0-\tau)]\right\} \tag{22}$$

with $s=1/\tau_c-i\pi/T$ and Re denotes the real part of. The second integral on the right-hand side may be considered as a Laplace transform with a periodic argument and Laplace variable s. Using the properties of the Laplace transform of periodic functions,[25] the upper limit of the second integral (∞) can be set to the period T according to

$$J_{20}(T)=A\frac{1}{1-\exp(-Ts)}$$
$$\times\frac{1}{T}\int_0^T dt_0\ \mathrm{Re}\int_0^T d\tau\exp(-s\tau)$$
$$\times\exp\left\{i\pi\frac{1-\delta}{2\delta}[S(t_0)-S(t_0-\tau)]\right\}. \tag{23}$$

This equation can be integrated using the analytical expression of the periodic function $S(t)$, i.e., Eqs. (5) and (6). After some tedious, but straightforward, algebra the final expression of the spectral density $J_{20}(T)$ reads

$$J_{20}(T)=A\tau_c\left\{1-\frac{\tau_p}{T}\left[\frac{(\pi\tau_c/\tau_p)^2}{1+(\pi\tau_c/\tau_p)^2}\right]\right\}$$
$$-\frac{A\tau_c^2}{T}\left\{\tanh\left(\frac{T}{2\tau_c}\right)+\frac{\sinh[(T-2\tau_p)/2\tau_c]}{\cosh(T/2\tau_c)}\right\}$$
$$\times\left\{1-\frac{2}{1+(\pi\tau_c/\tau_p)^2}+\frac{1-(\pi\tau_c/\tau_p)^2}{[1+(\pi\tau_c/\tau_p)^2]^2}\right\}. \tag{24}$$

In the limit of δ-function pulses, this expression can considerably be simplified,

$$J_{20}(T)=A\tau_c\left[1-\frac{2\tau_c}{T}\tanh\left(\frac{T}{2\tau_c}\right)\right], \tag{25}$$

and in the limit of zero-pulse spacing, one recovers the continuous spin-lock equation

$$J_{20}(T=\tau_p)=A\frac{\tau_c}{1+(\pi\tau_c/T)^2}=J_{20}(2\omega_1). \tag{26}$$

If the correlation time τ_c is much shorter than the cycle time T, the spectral density $J_{20}(T)$ reduces to the value at zero frequency, $J_0(0)=A\tau_c$.

The two limiting cases of the spectral density function $J_{20}(T)$ [Eqs. (25) and (26)] are compared in Fig. 2 as a function of the normalized frequency τ_c/T. Both functions show a similar frequency behavior. Due to the pulsed irradiation J_{20} takes a somewhat smaller value and the corresponding dispersion extends over a little larger frequency range. The relative ratio depends on τ_c/T, but levels off at $\tau_c/T \geqslant 0.3$. However, this ratio never exceeds 18%. For a similar spectral density, the ratio τ_c/T should be of the same order of magnitude for both extreme cases.

The spectral density function has been calculated assuming a single-exponential correlation function. However, in many experimental situations several independent processes are involved in determining the loss of correlation of the quadrupolar interaction:

$$\langle F^*_{20}(t) F_{20}(t-\tau)\rangle = \sum_i A^i \exp(-\tau/\tau_c^i), \tag{27}$$

and according to Eq. (17) one obtains

$$J_{km}(T,m\omega_0) = \sum_i J^i_{km}(T,m\omega_0). \tag{28}$$

The conditions for the validity of the perturbation treatment are that changes in the density operator are small on the time scale of the lattice motions, $\langle \mathcal{H}^2_Q\rangle \tau_c^2 \ll 1$.[23] Furthermore, it is assumed that the characteristic relaxation times are much longer than the pulse cycle time. The latter assumption implies the condition $\langle \mathcal{H}^2_Q\rangle \tau_c T \ll 1$. It should be noted that pulse cycle time-dependent relaxation rates are observed if the correlation time is of the order of the pulse cycle time. In this situation both conditions are equivalent.

Several authors have derived Eq. (24) before, although in a different manner and context. Rhim, Burum, and Elleman[10] and Vega and Vaughan[11] derived a full expression for dipolar relaxation in solids using the Magnus expansion to describe the periodic irradiation. The expression reported by the former authors is valid for pulses of arbitrary angle and pulse width. Furthermore, they state that to minimize spin-heating θ pulses with $\theta \ll \pi/2$ should be used. However, for spin $S = 3/2$ quadrupolar relaxation care must be exercised. For pulse angles $\theta \ll \pi/2$ the restriction to the secular terms involving $k + k' = 0$ in Eq. (11) may no longer be a good approximation which will invalid the present analysis. Recently, Vega, Poupko, and Luz reported a similar equation for spin $S = 1$ nuclei in a nonzero average quadrupolar interaction, modulated by exchange in a liquid-crystalline solvent.[14] They made use of the average Hamiltonian formalism and the results are in agreement with the complete line-shape analysis of the deuteron NMR spectrum. Furthermore, they analyzed the effect of the finite pulse width [Eq. (24) vs Eq. (25)].

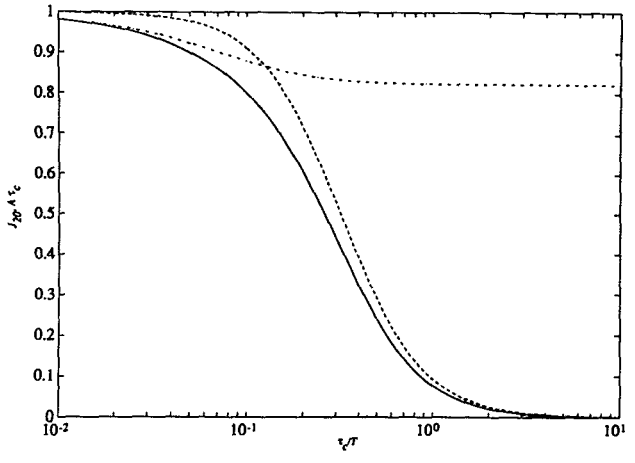

FIG. 2. Comparison of the two limiting spectral density functions Eqs. (25) and (26). Solid line: δ-function pulses limit. Dashed line: continuous spin-lock limit. Dotted-dashed line: relative ratio of the δ-function pulses and continuous spin-lock limits.

RELAXATION BEHAVIOR

Now, using the relaxation differential Eq. (16) and the properties of the spectral density function $J_{km}(T,m\omega_0)$, the evolution of the density operator Eq. (9) due to relaxation during the $(\pi/2)_x$ pulse train may be calculated. As shown before, the time dependence of the stroboscopically sampled density operator is analogous to $T_{1\rho}$ relaxation, but with spectral densities $J_{km}(T,m\omega_0)$ vs $J_{km}(k\omega_1 + m\omega_0)$. Taking the relevant Eq. (10) in Ref. 5, one obtains the time evolution at times $t_n = nT$ (in the RTTF)

$$\sigma^{**}(t_n) = 5^{1/2}[T_{10} f_{11}^{(\mathrm{qet})}(t_n) + T_{30} f_{31}^{(\mathrm{qet})}(t_n)] \tag{29}$$

with the relaxation functions

$$f_{11}^{(\mathrm{qet})}(t_n) = \tfrac{1}{5}[4\exp(R_3^{(\mathrm{qet})} t_n) + \exp(R_4^{(\mathrm{qet})} t_n)], \tag{30a}$$

$$f_{31}^{(\mathrm{qet})}(t_n) = \tfrac{2}{5}[-\exp(R_3^{(\mathrm{qet})} t_n) + \exp(R_4^{(\mathrm{qet})} t_n)], \tag{30b}$$

in which the superscript (qet) discerns relaxation during the quadrupolar echo train. The relaxation rates may be obtained from Eqs. (16) and (17) in Ref. 5, but with spectral densities $J_{km}(T,m\omega_0)$ vs $J_{km}(k\omega_1 + m\omega_0)$. Using the previously discussed approximation Eq. (20), the relaxation rates are given by

$$R_3^{(\mathrm{qet})} = -\left(\frac{eQ}{\hbar}\right)^2 [\tfrac{3}{4} J_{20}(T) + J_1(\omega_0) + \tfrac{1}{4} J_2(2\omega_0)], \tag{31a}$$

$$R_4^{(\mathrm{qet})} = -\left(\frac{eQ}{\hbar}\right)^2 [J_1(\omega_0) + J_2(2\omega_0)]. \tag{31b}$$

The $R_3^{(\mathrm{qet})}$ component contains the pulse cycle time-dependent spectral density $J_{20}(T)$.

It should be noted that the time evolution described by Eq. (29) refers to the RTTF interaction representation. However, the detection occurs in the rotating frame. Accordingly, the density operator has to be transformed back to the rotating frame. If the general form of the density operator in the RTTF is given by

$$\sigma^{**} = \sum_{l,m} b_{lm} T_{lm}, \tag{32}$$

then in the rotating frame the density operator reads

$$\sigma^{*}(t_n) = \sum_{k,l,m} b_{lm} T_{lk} D^{(l)}_{km}\left[0,\pi/2,\int_0^{t_n} dt'\,\omega_1(t')\right]. \tag{33}$$

Backtransforming Eq. (29) to the rotating frame by using Eqs. (32) and (33) yields the result

$$\sigma^*(t_n)=\sigma^*(t_n,p=\pm 1)+\sigma^*(t_n,p=\pm 3) \tag{34}$$

with

$$\sigma^*(t_n,p=\pm 1)=(\tfrac{5}{2})^{1/2}[(T_{1-1}-T_{1+1})f_{11}^{(\mathrm{qet})}(t_n)] - (\tfrac{3}{8})^{1/2}(T_{3-1}-T_{3+1})f_{31}^{(\mathrm{qet})}(t_n), \tag{35a}$$

$$\sigma^*(t_n,p=\pm 3)=\tfrac{5}{4}(T_{3-3}-T_{3+3})f_{31}^{(\mathrm{qet})}(t_n), \tag{35b}$$

which represent order $p=\pm 1$ single- and $p=\pm 3$ triple-quantum coherences, respectively.

Of course, in Ref. 5 exactly similar relaxation expressions were reported, but for the continuous spin-lock case. Due to relaxation during the quadrupolar echo pulse train, triple-quantum coherences are generated. In the extreme narrowing limit, the rates $R_3^{(\mathrm{qet})}$ and $R_4^{(\mathrm{qet})}$ have the same value and the relaxation becomes monoexponential. Moreover, in this situation the function $f_{31}^{(\mathrm{qet})}(t_n)$ equals zero for all times and no triple-quantum coherences will be excited. The advantage of the pulsed experiment is that the signal can be sampled between the pulses. In this experimental arrangement, the triple-quantum coherences are not observable. However, the triple-quantum coherences may be detected by a method analogous to the previously described $T_{1\rho}$ experiment with coherence transfer ($T_{1\rho}$CT).[5] In this experiment, after the $(\pi/2)_x$ pulse train an additional $(\pi/2)$ coherence transfer pulse is applied to convert the $T_{3\pm 3}$ coherences into $T_{3\pm 1}$ coherences. The latter coherences evolve into observable $T_{1\pm 1}$ coherences due to transverse relaxation during detection after the pulse sequence. The separation of coherence orders can be established by time proportional phase incrementation of the last $(\pi/2)$ coherence transfer pulse.

If the signal is sampled at the echo positions at times $t_n=nT$, only the $T_{1\pm 1}$ coherences are observable. According to Eq. (35a), the observed signal is represented by

$$s(t_n)=f_{11}^{(\mathrm{qet})}(t_n). \tag{36}$$

The relaxation is biexponential [Eq. (30a)]. The relative ratio of the fast and slowly relaxing components is 0.8:0.2, respectively. The relaxation rate of the fast relaxing component may be sensitive to the pulse spacing. The slowly relaxing component is determined by the spectral density at one and two times the Larmor frequency with respect to the static field, and, hence, does not give information about slowly fluctuating processes.

At the cost of spectrometer time, the triple-quantum coherences may be monitored by applying an additional coherence transfer pulse after the $(\pi/2)_x$ pulse train. Now the total pulse sequence reads

$$(\pi/2)_y-[T/2-(\pi/2)_x-T/2]_n - (\pi/2)_{\varphi-\pi/2}-t_2,\text{detection} \tag{37}$$

in which the number of pulses n is incremented. The phase φ is defined as a positive angle with respect to the $+y$ axis.[5] The separation of coherence orders can be established by time (i.e., number of pulses) proportional phase incrementation[26,27] (TPPI) of the last pulse of the sequence: $\varphi=n\Delta\varphi^{\mathrm{TPPI}}$. It should be noted that detection occurs after the pulse train. The last coherence transfer $(\pi/2)_{\varphi-\pi/2}$ pulse converts the generated triple-quantum coherences, Eq. (35b), into $T_{3\pm 1}$ coherences. The latter coherences evolve into detectable $T_{1\pm 1}$ coherences due to transverse relaxation during the detection period.

This experiment is exactly similar to the previous described $T_{1\rho}$CT experiment, but with a pulsed spin-lock field. The relevant expressions representing the signal contributions in the $T_{1\rho}$CT experiment are given by Eqs. (36) and (37) in Ref. 5. Changing the superscript (ρ) into (qet) to discern relaxation during the quadrupolar echo train, one obtains

$$s(t_n,t_2,p=\pm 1)=[\tfrac{1}{2}f_{11}^{(\mathrm{qet})}(t_n)f_{11}^{(1)}(t_2)+(6^{1/2}/32) \times f_{31}^{(\mathrm{qet})}(t_n)f_{13}^{(1)}(t_2)]\exp(\mp i\varphi), \tag{38a}$$

$$s(t_n,t_2,p=\pm 3)=-\tfrac{5}{32}6^{1/2}f_{31}^{(\mathrm{qet})}(t_n)f_{13}^{(1)}(t_2)\exp(\mp 3i\varphi), \tag{38b}$$

in which $\varphi=n\Delta\varphi^{\mathrm{TPPI}}$ is the phase defined in Eq. (37). For the sake of completeness the relaxation functions during the detection period are given by[7]

$$f_{11}^{(1)}(t_2)=\tfrac{1}{5}[3\exp(R_1^{(1)}t_2)+2\exp(R_2^{(1)}t_2)], \tag{39a}$$

$$f_{13}^{(1)}(t_2)=(6^{1/2}/5)[\exp(R_1^{(1)}t_2)-\exp(R_2^{(1)}t_2)] \tag{39b}$$

with rates

$$R_1^{(1)}=-\left(\frac{eQ}{\hbar}\right)^2[J_0(0)+J_1(\omega_0)], \tag{40a}$$

$$R_2^{(1)}=-\left(\frac{eQ}{\hbar}\right)^2[J_1(\omega_0)+J_2(2\omega_0)]. \tag{40b}$$

The superscript (1) denotes transverse relaxation. The signals have to be detected as a function of the number of pulses n, and, hence, a true two-dimensional (2D) experiment with TPPI has to be performed. Since the signals corresponding to $\pm p$ coherences have equal amplitudes, a real Fourier cosine transformation results in a pure adsorption spectrum. It is clear that the direct sampling method takes much less spectrometer time. However, in case of a short pulse spacing, due to electronic limitations, the direct sampling method may not be feasible. In this situation the 2D experiment may be a useful alternative.

EXPERIMENT

Quadrupolar echo train experiments have been performed on spin $S=3/2$ ^{23}Na in a sodium poly-(methylacrylate) ion-exchange resin. In a previous communication, the same resin has been investigated by a 2D $T_{1\rho}$CT experiment.[8] It was shown that the line shapes and relative intensities of the single- and triple-quantum signals are in agreement with the theoretical expressions based on the density operator calculations. However, in the ion-exchange resin, the spectral density at two times the precession frequency with respect to the spin-lock field $2\omega_1=209.4\times 10^3$ rad/s equals the value at zero frequency. The latter value has been obtained from transverse relaxation experiments. It was concluded that the spectral density does not show a dispersion in the frequency range 0–30 kHz. Accordingly, any cycle time dependence of the relaxation rates is not observed. The present system is still a suitable candidate to check the similarity of the $T_{1\rho}$ and quadrupolar echo train experiments. Furthermore, the validity of the relaxation rate expressions, Eqs.

(31a) and (31b), can be checked, since all relevant spectral densities are known.

The poly-(methylacrylate) ion-exchange resin, cross linked with 4.5% divinylbenzene (Zerolit 226) was obtained from BDH Chemicals Ltd, Poole, United Kingdom. The resin is completely neutralized with alkali (Merck) and immersed in water. The sodium capacity is 5×10^{-3} mole per gram resin, whereas the sodium content in the surrounding water medium is negligible. The experiments were performed on a Bruker MSL-400 spectrometer, at a static field strength of 9.4 T. To achieve a homogeneous H_1 field, a high-power probe (Bruker Z-34-v-HP) equipped with a solenoid was used. The temperature was controlled at 298 K using a gas thermostat. A series of experiments with different cycle times and two different H_1 field strength levels has been performed. The signal was sampled between the pulses. Furthermore, an experiment with an additional coherence transfer pulse after the $(\pi/2)_x$ pulse train (for ease of reference referred to as QET-CT) has been carried out. This experiment is similar to the previously reported $T_{1\rho}$CT experiment, but with a pulsed spin-lock field. For more experimental details concerning the 2D data analysis and separation of coherence orders the reader is referred to Ref. 8.

First, the results obtained with the direct sampling method will be presented. A typical quadrupolar echo train decay curve is displayed in Fig. 3. Note the logarithmic intensity scale. The solid line represents a fit of the data to a sum of two exponentials, in which the rates as well as the amplitude fractions were optimized. Parameters resulting from this fit are collected in Table I. Results obtained from experiments with different settings of the cycle time T and the pulse width τ_p are also presented in Table I. From Fig. 3 it is clear that a sum of two exponentials describes the data well. According to Eqs. (30a) and (36), the theoretical amplitude fractions of the fast and slowly relaxing components

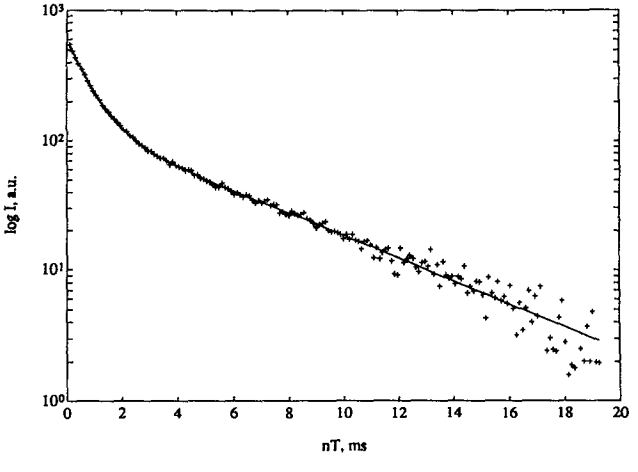

FIG. 3. Logarithm of the $(\pi/2)_x$ pulse train decay curve vs the sampling time $t_n = nT$. 175 echoes were sampled with a cycle time $T = 110\times10^{-6}$ s and pulse width $\tau_p = 10\times10^{-6}$ s. The solid line results from a nonlinear least-squares fit of the data to a sum of two exponentials. Fitted parameters are collected in Table I. Please note the pronounced biexponentiality.

TABLE I. Results of the quadrupolar echo train experiment in which the magnetization was sampled between the pulses. Relaxation rates and amplitude fractions of the fast and slow relaxing components result from the fit of the experimental decay curves to a sum of two exponentials. The cycle time T, the pulse width τ_p, and the duty cycle parameter $\delta = \tau_p/T$ are included too. (The estimated experimental reproducibility in $R_3^{(qet)}$ and $R_4^{(qet)}$ is 5% and 10%, respectively.)

T (10^{-6} s)	τ_p (10^{-6} s)	δ	$-R_3^{(qet)}$ (s^{-1})	Fraction	$-R_4^{(qet)}$ (s^{-1})	Fraction
60	10	0.17	1290	0.80	168	0.20
110	10	0.09	1270	0.79	179	0.21
210	10	0.05	1260	0.79	190	0.21
65	15	0.23	1340	0.77	199	0.23
115	15	0.13	1300	0.78	193	0.22
215	15	0.07	1260	0.79	190	0.21

are 0.8 and 0.2, respectively. The fitted amplitude ratios (Table I) are in close agreement, irrespective of the values of the cycle time T or pulse width τ_p.

The experimental reproducibility of the rates $R_3^{(qet)}$ and $R_4^{(qet)}$ is 5% and 10%, respectively. The reproducibility of the rate $R_4^{(qet)}$ is somewhat poor, due to the relatively small corresponding amplitude fraction (0.2 vs 0.8). Within experimental accuracy, the rates obtained with the different experimental settings are all equal. There is no cycle time and/or pulse-width dependence. In the present duty cycle range $0<\delta<0.23$, the effect of the finite pulse duration on the spectral density function $J_{20}(T)$ does not exceed the estimated experimental error margin 5%, irrespective of the correlation time [Eq. (24) or Ref. 14]. Accordingly, a possible pulse-width dependence of the rate $R_3^{(qet)}$ is beyond detection. The absence of any cycle time dependence and the estimated values of the relaxation rates will be interpreted below. First, the results of the quadrupolar echo train with coherence transfer will be discussed.

Figure 4 displays the ^{23}Na multiple-quantum spectrum obtained using pulse sequence Eq. (37) with TPPI of the last coherence transfer pulse. The spectrum results from a real cosine transformation with respect to $t_n = nT$ (F_1 dimension) after Fourier transformation with respect to the detection time t_2 (F_2 dimension). The section along the F_1 dimension at the exact resonance position in F_2 is displayed. The experimental parameters are $T = 60\times10^{-6}$ s, $\tau_p = 10\times10^{-6}$ s, and $\Delta\varphi = \pi/4$. Using this phase increment, the corresponding frequency shift between succeeding coherence orders equals $\Delta\varphi/2\pi T = 2.083$ kHz. Accordingly, the feature at 2.083 kHz is the single-quantum signal, whereas the signal at three times this frequency represents the triple-quantum contribution. It is clear that, just as in case of continuous spin-locking, due to relaxation during the $(\pi/2)_x$ pulse train triple-quantum coherences are generated.

The single- and the triple-quantum signal contributions are both fitted to a sum of two Lorentzians. Using a nonlinear least-squares procedure, the linewidths as well as the relative amplitude fractions (i.e., areas) were optimized. Results are collected in Table II, together with the previously reported results obtained with a $T_{1\rho}$CT experiment. There is

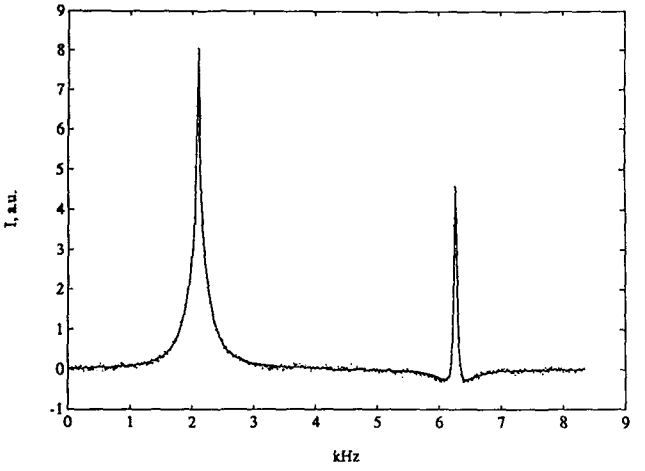

FIG. 4. ^{23}Na multiple-quantum spectrum resulting from the QET-CT experiment [pulse sequence Eq. (37)]. The section along the F_1 dimension (Fourier transform with respect to $t_n = nT$) at the resonance position in F_2 is displayed. The feature on the right-hand side represents the triple-quantum coherence. Experimental parameters: $T = 60\times10^{-6}$ s, $\tau_p = 10\times10^{-6}$ s, and the time-proportional phase increment $\Delta\varphi^{\mathrm{TPPI}} = \pi/4$. The solid line represents a nonlinear least-squares fit of a sum of two Lorentzians to both signal contributions. Parameters resulting from the fit are collected in Table II.

close agreement between the results obtained with the continuous and pulsed spin-lock experiments, respectively.

According to Eqs. (30b) and (38b) the triple-quantum signal broad and narrow components have equal amplitudes, but opposite signs. The experimental values (Table II) are in reasonable agreement. For the single-quantum signal contribution this amplitude ratio is somewhat more involved [Eq. (38a)] and depends on the transverse relaxation during the detection period t_2 (characterized by rates $R_1^{(1)}$ and $R_2^{(1)}$). For a discussion of the single-quantum signal broad- and narrow-component amplitude ratio the reader is referred to Ref. 8. Finally, if the triple-quantum contribution is divided by a factor of 5 and added to the single-quantum signal, the resulting line shape consists of two components with relative intensity ratio 0.8:0.2 [Eqs. (30a), (38a), and (38b)]. Fit parameters resulting from this combination are also collected in Table II and, again, the fitted amplitude fractions are in reasonable agreement.

It should be noted that the coherence transfer experiments are much more time consuming compared to the direct sampling method. Accordingly, in the QET-CT experiment the reproducibility is somewhat worse (10%), due to fact that less scans were accumulated (typically 16 vs 64). Averaged values of the relaxation rates are collected in Table III. Within statistical spread, no difference in relaxation rates originating from the different experimental methods can be detected.

Now, the relaxation rates will be interpreted in terms of the dynamic processes involved. According to Eq. (31b) and Eq. (17) in Ref. 5, the rates $R_4^{(\mathrm{qet})}$ and $R_4^{(\rho)}$ are sensitive to the spectral densities at one and two times the Larmor frequency with respect to the static field H_0. These relaxation rates should be equal to the rate $R_2^{(1)}$ extracted from the slowly relaxing component of the transverse relaxation curve. The latter rate has the value $R_2^{(1)} = -197\ \mathrm{s}^{-1}$, which is in reasonable agreement with the values of $R_4^{(\mathrm{qet})}$ and $R_4^{(\rho)}$.

As was discussed before, in the ion-exchange resin, the spectral density function does not show a dispersion in the region 0–30 kHz. Accordingly, the characteristic correlation times describing the fluctuating quadrupolar interaction are at least one order of magnitude smaller than the value, say, 30×10^{-6} s. With the present experimental pulse timing, the characteristic correlation times τ_c^j are much smaller compared to the cycle times T (Table I). According to Eq. (24), in the limit $\tau_c^j \ll T$ the spectral density function $J_{20}(T)$ equals the value at zero frequency $J_0(0)$. Furthermore, in this limit no cycle time and/or pulse-width dependence can be observed. This is in accordance with the experimental results, even in the limit of continuous spin-locking ($\delta \to 1$). If $J_{20}(T) = J_0(0)$, the rate $R_3^{(\mathrm{qet})}$ can be calculated using the estimated spectral densities at zero, one, and two times the Larmor frequency ω_0. The products of the latter spectral density functions and the coupling constant have been estimated from extensive field-dependent longitudinal and transverse relaxation experiments.[28] Inserting the values $(eQ/\hbar)^2 J_0(0) = 1530\,\mathrm{s}^{-1}$, $(eQ/\hbar)^2 J_1(\omega_0) = 116\,\mathrm{s}^{-1}$,

TABLE II. Results of the 2D quadrupolar echo pulse train with an additional coherence transfer pulse, Eq. (37) (QET-CT). For comparison, the results of the previously reported $T_{1\rho}$CT experiment on the same resin have been included too. Relaxation rates and amplitude fractions of the broad and narrow components result from the fit of the line shapes to a sum of two Lorentzians. In the QET-CT experiment, $T = 60\times10^{-6}$ s, pulse width $\tau_p = 10\times10^{-6}$ s, and the duty cycle parameter $\delta = \tau_p/T = 0.17$. The $T_{1\rho}$CT experiment is performed with a somewhat lower H_1 field-strength level: $\omega_1 = 104.7\times10^3$ rad/s. [The superscript (*) denotes (qet) and (ρ) for the QET-CT and the $T_{1\rho}$CT experiment, respectively.]

Signal	$-R_3^{(*)}$ (s^{-1})	Fraction	$-R_4^{(*)}$ (s^{-1})	Fraction
QET-CT $s(p=\pm1)$	1240	0.83	171	0.17
$s(p=\pm3)$	1350	−0.96	188	1.04
$s(p=\pm1)+\frac{1}{5}s(p=\pm3)$	1230	0.78	174	0.22
$T_{1\rho}$CT[a] $s(p=\pm1)$	1230	0.86	181	0.14
$s(p=\pm3)$	1310	−0.98	185	1.02
$s(p=\pm1)+\frac{1}{5}s(p=\pm3)$	1220	0.81	182	0.19

[a] Results taken from Ref. 8. The experimental reproducibility in the relaxation rates is 10%.

TABLE III. Compilation of relaxation rates obtained by the different experimental methods.

	$-R_3^{(*)}$ (s^{-1})	$-R_4^{(*)}$ (s^{-1})
QET[a]	1290 ± 30	185 ± 10
QET-CT[b]	1300 ± 80	180 ± 10
$T_{1\rho}CT$[c]	1270 ± 60	183 ± 3

[a] Averaged rates obtained by the QET experiments with different experimental cycle times and pulse widths.
[b] Rates originating from the QET-CT experiment after averaging the $s(p=\pm 1)$ and $s(p=\pm 3)$ signal contributions.
[c] The corresponding values from the $T_{1\rho}$CT experiment.

and $(eQ/\hbar)^2 J_2(2\omega_0) = 81\ s^{-1}$ into Eq. (31a), one obtains $R_3^{(qet)} = -1280\ s^{-1}$. The latter value agrees closely with those obtained from the $T_{1\rho}$ and quadrupolar echo train experiments.

CONCLUSIONS

For spin $S = 3/2$ the time evolution of the density operator under the $(\pi/2)_x$ pulse train has been analyzed as a function of the pulse cycle time and pulse width. It has been shown that outside the extreme narrowing limit the relaxation is biexponential. The amplitude ratio of the fast and slowly relaxing component equals 0.8:0.2. The rate of the fast relaxing component gives access to a spectral density function which is cycle time dependent in the presence of slowly fluctuating processes. Furthermore, due to relaxation under the effect of the quadrupolar echo train triple-quantum coherences may be excited. The latter coherences can be monitored using a 2D experiment with an additional coherence transfer pulse after the $(\pi/2)_x$ pulse train. The various theoretical expressions have been checked in an experimental study of sodium in an ion-exchange resin. Although the present system does not show any cycle time-dependent relaxation rates, for spin $S = 3/2$ the similarity of the $T_{1\rho}$ and the quadrupolar echo train experiment has been confirmed. The spectral density function does not show a dispersion in the relevant frequency range 0–30 kHz. Accordingly, the extracted relaxation rates agree with the spectral densities obtained from conventional longitudinal and transverse relaxation experiments.

The present formalism allows straightforward incorporation of additional relaxation mechanisms by extending the fluctuating Hamiltonian Eq. (2) accordingly. The spectral density function has been calculated assuming an exponential correlation function. Other models of the electric-field-gradient temporal behavior can be taken into account by inserting the relevant correlation function into Eq. (17).

As mentioned before, the relaxation under the quadrupolar echo train pulse sequence is very similar to $T_{1\rho}$ relaxation. However, there are some important differences. Although most of the differences are well known, the main advantages of the quadrupolar echo train experiment will be summarized.

(i) Very fast data acquisition due to the fact that the complete relaxation curve is recorded in one scan.

(ii) Well-defined ratio of the fast and slowly relaxing component (0.8:0.2). In the continuous spin-lock experiment using direct detection the corresponding ratio is somewhat complicated, due to the presence of an interference term [Eq. (31) in Ref. 5].

(iii) The cycle time can easily be varied. The limiting factor is the electronic dead time of the spectrometer receiver. In the spin-lock experiment, the corresponding experimental parameter is the H_1 field-strength level. Although, this level can be varied by adopting the transmitter power, a simultaneous power level and phase switch between the preparation pulse and the spin-lock field is electronically difficult to achieve. Of course, the continuous spin-lock experiment has its merits too.

(iv) For a similar spectral density J_{20}, in the pulsed and continuous spin-lock experiment the frequency $1/T$ should be of the same order of magnitude (Fig. 2). In this case the power ratio equals $P(\mathrm{QET})/P(T_{1\rho}) \approx T/\tau_p$. It is clear that the pulsed experiment takes more power especially in the limit of a small pulse duration.

(v) To study relatively more rapidly fluctuating quadrupolar interactions, one needs very short cycle times and, accordingly, the continuous spin-lock experiment with a high H_1 field is still the best experimental approach.

(vi) The spin-lock experiment is sensitive to the value of the spectral density at frequency $2\omega_1$, irrespective of the actual shape of the correlation function.

The chosen experimental approach will clearly depend on the kind of system to be investigated and the electronic performance of the spectrometer.

ACKNOWLEDGMENTS

J. G. Hollander is gratefully thanked for help with the experiments. Thanks are due to R. H. Tromp for providing a full set of relaxation data from which the spectral densities at zero, one, and two times the Larmor frequency were calculated. Professor J. C. Leyte and Dr. J. de Bleijser are gratefully acknowledged for helpful discussions.

APPENDIX

In this appendix it will be shown that in the relaxation master equation the terms involving odd values of $k + k'$ vanish. With the restriction to the secular terms with $m = -m'$ but without the condition $k + k' = 0$, and neglecting the imaginary part of the spectral density function, the relaxation master Eq. (11) reads

$$\frac{d\sigma^{**}}{dt} = -C^2 \sum_{k,k'=-2}^{2} \exp\left[i(k+k')\int_0^t dt'\,\omega_1(t')\right] \times [T_{2k},[T^{\dagger}_{2-k'},\sigma^{**}]] \sum_{m=-2}^{2} d^{(2)}_{km}(-\pi/2) \times d^{(2)}_{-k'm}(-\pi/2)\frac{1}{2}\int_{-\infty}^{\infty} d\tau \langle F^{*}_{2m}(t)F_{2m}(t-\tau)\rangle \times \exp\left\{i\left[m\omega_0\tau - k'\int_{t-\tau}^{t} dt'\,\omega_1(t')\right]\right\}. \quad \text{(A1)}$$

According to Eqs. (14), (19), and (20), for $m \neq 0$ the spectral density function has the symmetry property

$$\frac{1}{2}\int_{-\infty}^{\infty} d\tau \langle F^{*}_{2m}(t)F_{2m}(t-\tau)\rangle \exp\left\{i\left[m\omega_0\tau - k'\int_{t-\tau}^{t} dt'\,\omega_1(t')\right]\right\} \approx J_m(m\omega_0) = J_{-m}(-m\omega_0), \quad m\neq 0. \tag{A2}$$

The reduced Wigner matrix elements obey the symmetry relation[22]

$$d^{(2)}_{km}(-\pi/2) = (-1)^k d^{(2)}_{k-m}(-\pi/2). \tag{A3}$$

Together with Eqs. (A2) and (A3), the relaxation master Eq. (A1) can be expressed as

$$\frac{d\sigma^{**}}{dt} = -C^2 \sum_{k',k=-2}^{2} \exp\left[i(k+k')\int_0^t dt'\,\omega_1(t')\right][T_{2k},[T^{\dagger}_{2-k'},\sigma^{**}]] \times \sum_{m=0,1,2} [1+(-1)^{k+k'}(1-\delta_{m0})]d^{(2)}_{km}(-\pi/2)d^{(2)}_{-k'm}(-\pi/2) \times \frac{1}{2}\int_{-\infty}^{\infty} d\tau \langle F^{*}_{2m}(t)F_{2m}(t-\tau)\rangle \exp\left\{i\left[m\omega_0\tau - k'\delta_{m0}\int_{t-\tau}^{t} dt'\,\omega_1(t')\right]\right\} \tag{A4}$$

with δ_{m0} the Kronecker delta function. The terms with $m\neq 0$ and odd values of $k+k'$ are seen to vanish. With $m=0$ the terms involving odd values of $k+k'$ vanish due to the fact that $d^{(2)}_{k0}(-\pi/2)$ equals zero for odd k [Eq. (A3)].

[1] C. J. M. van Rijn, J. de Bleijser, and J. C. Leyte, J. Phys. Chem. **93**, 5284 (1989); J. Breen, L. Huis, J. de Bleijser, and J. C. Leyte, Ber. Bunsenges. Phys. Chem. **92**, 160 (1988).
[2] A. Delville, P. Laszlo, and R. Schyns, Biophys. Chem. **24**, 121 (1986); L. van Dijk, M. L. H. Gruwel, W. Jesse, J. de Bleijser, and J. C. Leyte, Biopolymers **26**, 261 (1987).
[3] D. Petit and J.-P. Korb, Phys. Rev. B **37**, 5761 (1988).
[4] S. Forsen, T. Drakenberg, and H. Wennerström, Q. Rev. Biophys. **19**, 83 (1987).
[5] J. R. C. van der Maarel, J. Chem. Phys. **91**, 1446 (1989).
[6] F. Lurçat, Comptes Rendus **240**, 2517 (1955); J. Pekar and J. S. Leigh, J. Magn. Reson. **69**, 582 (1986).
[7] G. Jaccard, S. Wimperis, and G. Bodenhausen, J. Chem. Phys. **85**, 6282 (1986).
[8] J. R. C. van der Maarel, R. H. Tromp, J. C. Leyte, J. G. Hollander, and C. Erkelens, Chem. Phys. Lett. **169**, 585 (1990).
[9] W. Gründer, H. Schmiedel, and D. Freude, Ann. Phys. 7 Folge **27**, 409 (1971).
[10] W.-K. Rhim, D. P. Burum, and D. D. Elleman, J. Chem. Phys. **68**, 692 (1978).
[11] A. J. Vega and R. W. Vaughan, J. Chem. Phys. **68**, 1958 (1978).
[12] M. Mehring, *Principles of High Resolution NMR in Solids*, 2nd ed. (Springer, Berlin, 1983).
[13] J. S. Blicharski, Can. J. Phys. **64**, 733 (1986).
[14] A. J. Vega, R. Poupko, and Z. Luz. J. Magn. Reson. **83**, 111 (1989).
[15] D. Lankhorst, J. Schriever, and J. C. Leyte, J. Magn. Reson. **51**, 430 (1983).
[16] J. R. C. van der Maarel, Chem. Phys. Lett. **155**, 288 (1989).
[17] J. S. Blicharski, Acta Phys. Polon. A **41**, 223 (1972).
[18] U. Haeberlen and J. S. Waugh, Phys. Rev. **185**, 420 (1969).
[19] P. Mansfield, in *Progress in Nuclear Magnetic Resonance Spectroscopy*, edited by J. W. Emsley, J. Feeney, and L. H. Sutcliffe (Pergamon, Oxford, 1972), Vol. 8.
[20] J. McConnell, *The Theory of Nuclear Magnetic Relaxation in Liquids* (Cambridge University, Cambridge, 1987).
[21] H. W. Spiess, in *N. M. R., Basic Principles and Progress*, edited by P. Diehl (Springer, Berlin, 1978), Vol 15.
[22] M. E. Rose, *Elementary Theory of Angular Momentum* (Wiley, New York, 1957).
[23] A. Abragam, *Principles of Nuclear Magnetism* (Oxford University, Oxford, 1961).
[24] L. G. Werbelow, J. Chem. Phys. **70**, 5381 (1979).
[25] *Handbook of Mathematical Functions*, edited by M. Abramowitch and I. A. Stegun (Dover, New York, 1972).
[26] R. R. Ernst, G. Bodenhausen, and A. Wokaun, *Principles of Nuclear Magnetic Resonance in One and Two Dimensions* (Oxford University, Oxford, 1987).
[27] M. Munowitz and A. Pines, *Advances in Chemical Physics*, edited by I. Prigogine and S. A. Rice (Wiley, New York, 1987), Vol. LXVI.
[28] R. H. Tromp, J. R. C. van der Maarel, J. de Bleijser, and J. C. Leyte (unpublished).